Nuclear Engineering and Technology 52 (2020) 2613–2619

Contents lists available at ScienceDirect

Nuclear Engineering and Technology

journal homepage: www.elsevier.com/locate/net

Original Article

Gamma radiation shielding properties of poly (methyl methacrylate) / Bi_2O_3 composites

Da Cao, Ge Yang*, Mohamed Bourham, Dan Moneghan

Department of Nuclear Engineering, North Carolina State University, Raleigh, NC, 27695-7909, USA

ARTICLE INFO

Article history:
Received 31 December 2019
Received in revised form
18 April 2020
Accepted 25 April 2020
Available online 29 April 2020

Keywords:
Ultraviolet (UV) curing
Poly (methyl methacrylate)
Bi_2O_3 composites
Radiation shielding

ABSTRACT

This work investigated the gamma-ray shielding performance, and the physical and mechanical properties of poly (methyl methacrylate) (PMMA) composites embedded with 0–44.0 wt% bismuth trioxide (Bi_2O_3) fabricated by the fast ultraviolet (UV) curing method. The results showed that the addition of Bi_2O_3 had significantly improved the gamma shielding ability of PMMA composites. Mass attenuation coefficient and half-value layer were examined using five gamma sources (Cs-137, Ba-133, Cd-109, Co-57, and Co-60). The high loading of Bi_2O_3 in the PMMA samples improved the micro-hardness to nearly seven times that of the pure PMMA. With these enhancements, it was demonstrated that PMMA/Bi_2O_3 composites are promising gamma shielding materials. Furthermore, the fast UV curing exerts its great potential in significantly shortening the production cycle of shielding material to enable rapid manufacturing.

1. Introduction

Advanced radiation shielding materials play a critical role in many applications, including nuclear medical imaging and therapy, nuclear waste storage, space exploration, and high-energy physics experiments. Unwanted exposure to ionizing radiation could be biologically hazardous to both humans and the environment, as it can lead to organ damage, cell mutation, component failure, and other harmful effects. When photon type radiation, such as gamma rays, travel through matter, there are three major interactions that can occur: the photoelectric effect, Compton scattering, and pair production (for $E\gamma > 1.022$ MeV). All these processes lead to a partial or complete energy transfer from photons to electrons. Materials with a high atomic number (Z) have a better gamma shielding ability than lower Z materials due to their higher interaction probability with photons. To mitigate or eliminate the influence of gamma radiation, lead, copper, stainless steel, and other high-Z materials [1] have historically been applied as shielding materials. However, these traditional shielding materials are costly, heavy, and often toxic to the environment. There is an increasing demand for developing new radiation shielding materials that can attenuate both gamma rays and neutrons whilst mitigating the disadvantages of traditional shielding materials. During the past decade, high-Z nano- and micro-materials dispersed in polymer matrices have shown enhanced ability in attenuating and absorbing high energy radiation [2–4]. Due to the merits of lightweight and geometric conformability, plastic composites have been applied in medical fields for protecting humans from penetrative X-rays during radiotherapy [5,6]. Additional applications for reducing dose absorption onboard spacecraft and aircraft also have been developed for future space exploration and air travel [7,8].

For polymer composite fabrication, thermal polymerization is one of the frequently used methods, which usually occurs usually under high temperatures and could take hours or even days to complete [4,8]. In comparison, ultraviolet (UV) radiation-induced polymerization is a more efficient method, enabling the fast transformation of liquid resin into a solid material [9]. Its curing time can be reduced to several minutes, as opposed to a few hours or days for thermal polymerization. When comparing to other curing sources, e.g., gamma rays [10] and electron beams [11], UV curing requires a lower equipment investment and much less energy consumption. Normally, because of the limited penetration depth into the matter, UV curing is applied mostly in the fast drying of paints and adhesives, as well as optical disks [12]. Since the concentration of photoinitiator is an important factor for the UV curing process [9], 0.2 wt%-0.4 wt% of the photoinitiator is the optimal loading range for curing a thin film [9]. However, Udagawa et al. [13] added 2 wt%-3 wt% of photoinitiator into an epoxy resin

* Corresponding author.
E-mail address: gyang9@ncsu.edu (G. Yang).

https://doi.org/10.1016/j.net.2020.04.026

to obtain a maximum curing rate. Thus, it will be a good attempt to obtain a thicker shielding material taking just several minutes with utilizing a higher concentration of photoinitiator or higher intensity of UV source. In this paper, 0.94 g TPO photoinitiator, corresponding 6.9 wt%-12.3 wt% for samples containing 0 wt%- 44 wt% Bi_2O_3, was added into composites to achieve a faster polymerization.

Due to the well-known toxicity of lead (Pb) to the environment, bismuth (Bi) is being investigated as a potential replacement material in radiation shielding and playing a significant role in developing next-generation shielding materials with more desirable properties. Singh et al. have carried out a detailed study of the gamma attenuation and structural properties of bismuth/glass system [14–16]. Poly (methyl methacrylate) (PMMA), commonly known as "acrylic," has excellent optical clarity, good abrasion resistance, hardness, and stiffness. Though it has lower mechanical strength and gamma ray shielding ability than other metal shielding materials, it can be mixed with high-Z materials to improve the mechanical and shielding properties. Bela et al. [8] applied PMAA/colemanite (CMT) composite in gamma and neutron shielding experiments. They found CMT reinforcement of PMMA increased the radiation shielding capacity by 11.1% for Cs-137 gamma source and 38.56% for neutrons from Pu–Be neutron source. And they also showed PMMA/CMT composites have a better thermal stability than pure PMMA.

In this study, we apply the fast UV curing method in producing PMMA composite with 0–44.0 wt% Bi_2O_3. Systematic shielding experiments using the five gamma sources and micro-hardness measurements have been conducted to investigate the shielding and mechanical properties of these composites.

2. Experiments

2.1. Materials

Poly (methyl methacrylate) (-(-CH2=C (CH3) COOCH3-)n-, PMMA) and Methyl methacrylate, 99%, stab. (CH2=C (CH3) COOCH3, MMA) both supplied by Alfa Aesar (Tewksbury, USA). Diphenyl (2,4,6-trimethylbenzoyl)phosphine oxide ((CH3) 3C6H2COP(O)(C6H5)2, 97%, TPO) is obtained from Sigma Aldrich (Darmstadt, Germany). Bismuth Oxide (99.9% metal base, Bi_2O_3) purchased from Inframat Advanced Material company (Manchester, USA). The average size of Bi_2O_3 particles is 2–5 μm.

2.2. Preparation of PMMA composites

The PMMA composites were prepared by the UV curing method. As UV curing is either dependent on radical polymerization for acrylate-based resins or cationic polymerization for epoxies and vinyl ethers, the acrylate-based resin was used in this experiment, offering a shorter reaction time [9]. The UV curing machine is the B9 Model Cure from B9Creations, with the wavelength of the UV source between 390 and 410 nm. Diphenyl (2,4,6-trimethylbenzoyl) phosphine oxide(TPO) is applied as a photoinitiator to boost a photoreaction on the absorption of light initiating or catalyzing polymerization while it absorbs visible light from 350 to 420 nm [13].

The pre-polymerized PMMA beads, Bi_2O_3 particle (0 wt%, 15.6 wt%, 24.6 wt%, 34.3 wt%, and 44.0 wt%), and TPO photoinitiator were mixed together and poured into the MMA monomer liquid, then stirred slowly for several minutes to reduce air bubble inclusion. The added amount of TPO was 0.94 g for every sample when the weight ratio between PMMA and MMA is 3:7. The mixed solutions were then poured into the mold (60 mm (diameter) x 15 mm (height)) and placed into the curing machine. For each sample, the curing time is 9 min, with a distance of 6 cm from the UV source.

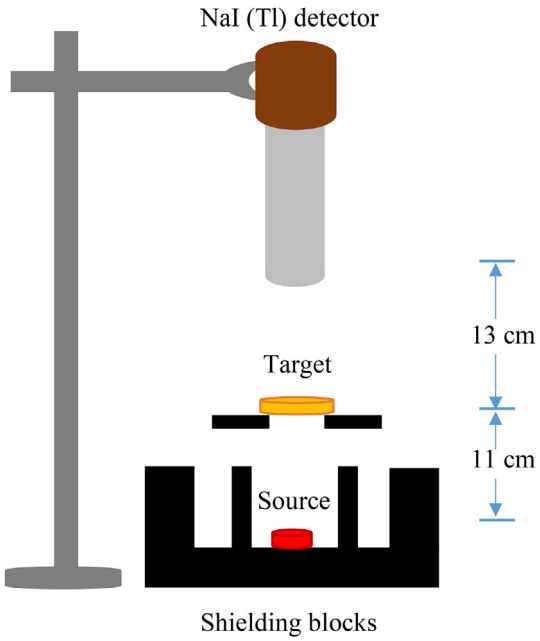

Fig. 1. Sketch diagram of gamma shielding setup.

2.3. Characterization

2.3.1. 3D X-ray tomography

Since the samples were too thick to be observed clearly with a regular optical microscope, a Zeiss Xradia 510 Versa 3D X-ray Tomography System was employed to check if Bi_2O_3 particles diffused homogeneously within the PMMA plastic. This equipment is a laboratory-based nanoscale 3D X-ray microscope enabling submicron imaging of samples from mm to inches, which allows us to observe Bi_2O_3 particles of several microns without the need to cut samples into a certain size.

2.4. Gamma shielding

The gamma shielding experiments were conducted using the setup shown in Fig. 1. The gamma radiation sources were stacked vertically as follows: Cs-137, Ba-133, Cd-109, Co-57 with 1 μCi activity, and Co-60 with 4.765 μCi activity, which emits gamma rays at 662 keV, 356 keV, 88 keV, 122 keV, and 1170 and 1330 keV, respectively. The total exposure time was 30 min. Sources were placed within the shielding lead block, which was surrounded by lead blocks for partial collimation. The sample was put on a ring plate 11 cm above from the source, while the NaI (Tl) detector with a Digi Base (ORTEC, 905 series) 13 cm above the base of the sample.

Generally, when monoenergetic gamma rays are collimated into a narrow beam and pass through a target with specific thickness before striking a detector, they will experience a simple exponential attenuation process. The probability per unit path length from removing gamma-ray photons of the beam after penetrating the target is the sum of three major interactions, described by Equation (1).

$$\mu\left(cm^{-1}\right) = \tau(photoelectric) + \sigma(Compton) + \kappa(\text{pair}) \quad (1)$$

The sum of these terms is called the linear attenuation coefficient (μ). Thus, the number of transmitted photons, I, can be given

in terms of the number without a target, I_0, as shown in Equation (2), where x is the target thickness [17].

$$I = I_0 \exp(-\mu x) \quad (2)$$

Furthermore, the thickness of the target where the intensity of incident gamma ray has been attenuated to 50% is known as the half-value layer (HVL) [17], which is shown by Equations (3) and (4).

$$0.5 I_0 = I_0 \exp(-\mu x) \quad (3)$$

$$x = 0.693/\mu \quad (4)$$

Once the linear attenuation coefficient has been obtained, the HVL can be easily calculated. Its value indicates the shielding efficiency against radiation. The lower the HVL, the smaller thickness will be used to attenuate the same kind of gamma radiation.

Considering the density of the target varies, directly using a linear attenuation coefficient is limited. Instead, the mass attenuation coefficient is often used to remove the dependence on density, ρ, which can be expressed as in Ref. [17].

$$\mu\left(cm^2/g\right) = \mu\left(cm^{-1}\right)/\rho\left(g/cm^3\right) \quad (5)$$

These three gamma shielding properties were obtained based on recording counts of each sample. For comparison, the sample with 0 wt% Bi_2O_3 was set as the reference.

2.5. Knoop hardness measurements

Micro-hardness tests were conducted on all samples to examine their mechanical hardness. A micro indentation system (Micromet 5103), made by Mitutoyo Corporation, was used for measuring Knoop hardness. Under a constant load, a pyramidal diamond indenter having a rhombic cross section and vertically opposite angles of 172.5° and 130° was pressed into the polished surface of the tested samples, and the projected area of the resulted indent was observed using an optical microscope [18]. The loading press in the lab can be set from 9.807×10^{-2} N–9.807 N. The Knoop hardness can be expressed by Equation (6).

$$H_K = 1.451F/d^2 \quad (6)$$

where d is the length of indent along its long axis, and F is the test force. In this experiment, the load is selected as H_K 0.01 (98.07×10^{-3} N) to achieve a clear indentation, which caused little destruction on the surface of samples.

3. Results and discussion

Fig. 2(a–c) shows the surface morphology of PMMA composite with 0 wt%, 15.6 wt%, and 44.0 wt% Bi_2O_3 addition. There are no observable particles on the surface of the pure PMMA composite. However, we observed an even distribution of particles, which dispersed more densely with the increasing loading in the case of the PMMA composites with 15.6 wt% and 44.0 wt% Bi_2O_3 addition.

When observing samples from the angle of 90 °C, there is an obvious stratification in the samples with 15.6 wt% to 44.0 wt% Bi_2O_3 addition, while the sample of 15.6 wt% Bi_2O_3 addition has a much more serious stratification. Fig. 3(a) shows a 3D model from a scan of 360° depicting the sample with a loading of 15.6 wt% Bi_2O_3 addition. The white color in the image indicates X-ray can easily penetrate the part with little attenuation, while the black color represents a much greater attenuation. Thus, it is reasonable to assume the black phase should be filled with Bi_2O_3 particles, since it has a higher density than PMMA matrix. The interesting phenomenon is that a layer with low-Z material (white phase) exists on the bottom of samples. The cross-section of both white and black phases, shown in Fig. 3 (b), reveals that Bi_2O_3 dispersed well whilst many particles with a larger diameter are distributed in the white layer. Though no detailed characteristic tests were applied to define this material, it should have less influence on gamma shielding owing to its low attenuation ability. A further study can be conducted to explore this special phenomenon in UV cured samples.

Following the homogeneity study of Bi_2O_3 particles, a series of gamma shielding experiments were conducted. Figs. 4–6 give the gamma shielding properties of PMMA composites with 0–44.0 wt% Bi_2O_3 particles under five gamma sources, in which the values of mass attenuation coefficient and HVL from PMMA/Bi_2O_3 shows the improvement than that of pure PMMA within 1000 keV range.

From Fig. 4, it is obvious that the mass attenuation coefficient (MAC) improves with increased loading of Bi_2O_3 particles at lower energy ranges. When the gamma energy is larger than 300 keV, the MAC of PMMA composites with Bi_2O_3 particles is still higher than the pure one; however, there exist fluctuations where the MAC is not improving proportionally with the increase of the loading of particles. This is possibly due to the partial homogeneity of samples when a stratification exists. Besides, the shielding ability of PMMA composite with the loading of Bi_2O_3 particles at lower gamma energy is better than that in higher gamma energy. This interesting phenomenon could be attributed to the well-observed trend that a lower probability of interaction occurs when the energy of gamma ray is higher. The peak around 100 keV should be the K-edge of Bi element at 90.5 keV [19] since the sample with 0 wt% Bi_2O_3 has no such peak around 100 keV [19].

Since HVL is simply obtained by dividing the linear attenuation coefficient, the corresponding trend is similar to that of Fig. 4. As shown in Fig. 5, the essential thickness of the pure PMMA sample is much larger than other PMMA composites with Bi_2O_3 addition to attenuate the intensity of gamma ray to 50% for gamma energy less than 1130 keV. For example, when gamma energy is 662 keV, the pure PMMA composite needs a thickness of around 38 cm to

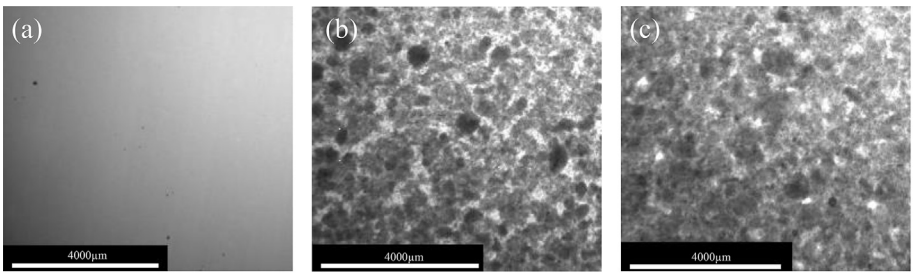

Fig. 2. The surface morphology of PMMA composites with (a) 0 wt%; (b) 15.6 wt% (c) 44.0 wt% Bi_2O_3 addition.

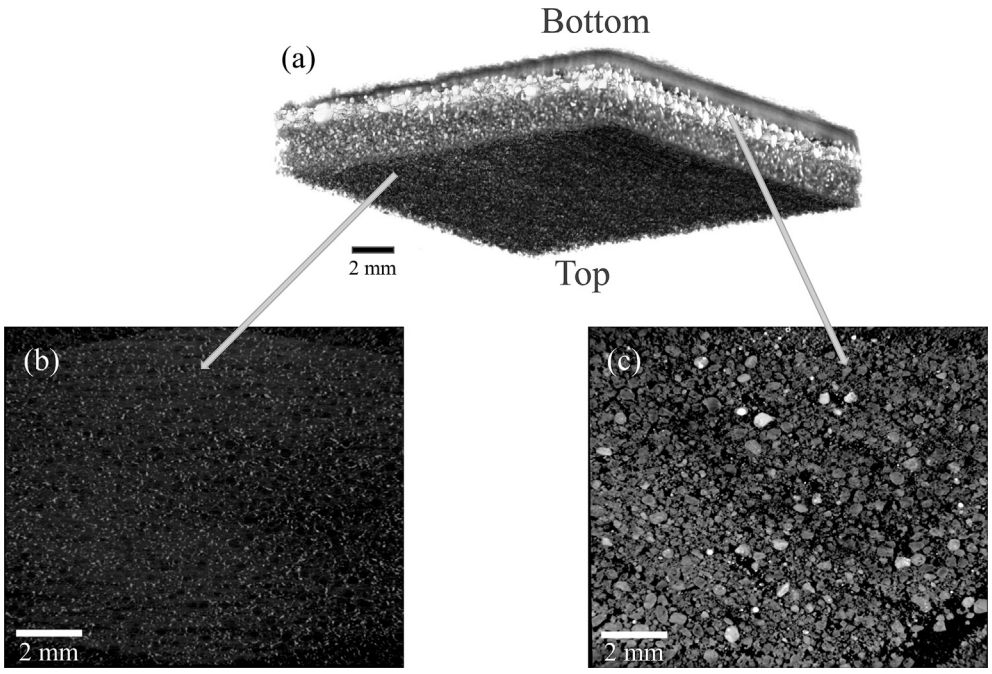

Fig. 3. (a) 3D tomography of PMMA composite with 15.6 wt% Bi2O3 addition; (b) cross section of the black phase; (c) cross section of the white phase.

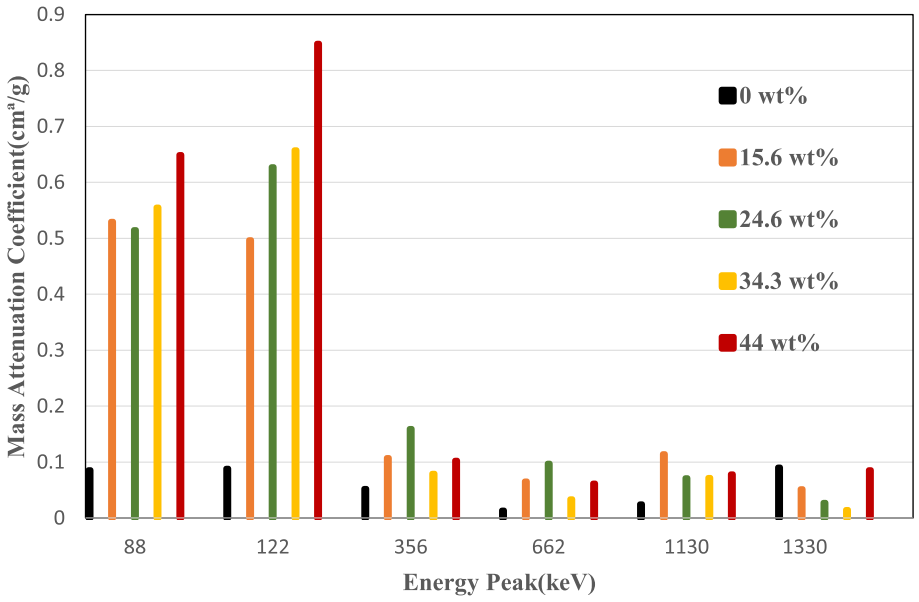

Fig. 4. Mass attenuation coefficient of PMMA composites with different loadings of Bi_2O_3.

decrease gamma ray to the half intensity while PMMA composite with 44.0 wt% Bi_2O_3 particles only need 5 cm. There is an unexpected tendency for gamma energy larger than 1130 keV. The underlying reason could be that the fewer counts in high energy or scatting problem because of the basic setup. These results indicate PMMA composites with Bi_2O_3 particles have a better gamma shielding ability than pure PMMA within the lower gamma energy range. It further demonstrates the important role of Bi_2O_3 particles in attenuating gamma rays.

Fig. 6 shows the experimental results of the mass attenuation coefficient and simulation results as well (using commercial MicroShield software). The corresponding curves of PMMA with Bi_2O_3 loadings from MicroShield also have a peak of around 100 keV. We noted that the simulation curves are much higher than experimental ones within the lower energy range, while in the higher energy, they are almost the same. The significant background noise in the low energy range may be the main cause of this phenomenon.

The Knoop micro-hardness results of PMMA composites with different concentrations of Bi_2O_3 particles are shown in Fig. 7. Each individual data point represents an average value that which is based on measurements of six different positions on the sample surface. The inset micrograph is taken from the indent of the sample surface, which clearly shows the rhombic cross section

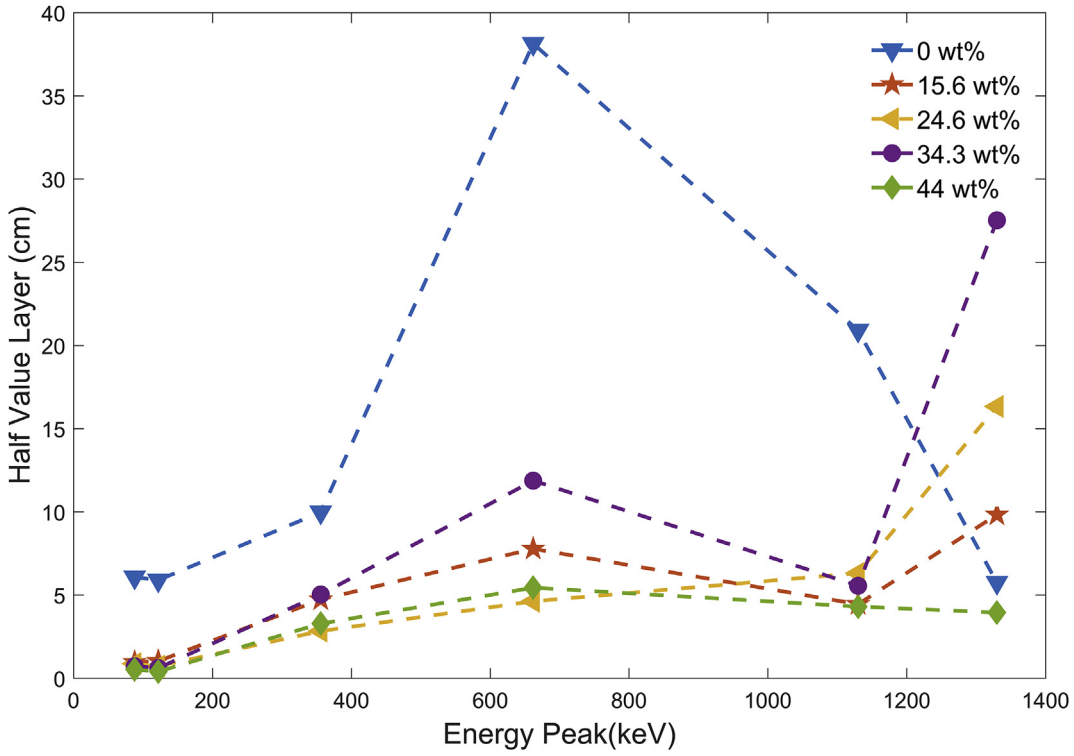

Fig. 5. Half value layer of PMMA composites with different loadings of Bi_2O_3 particles.

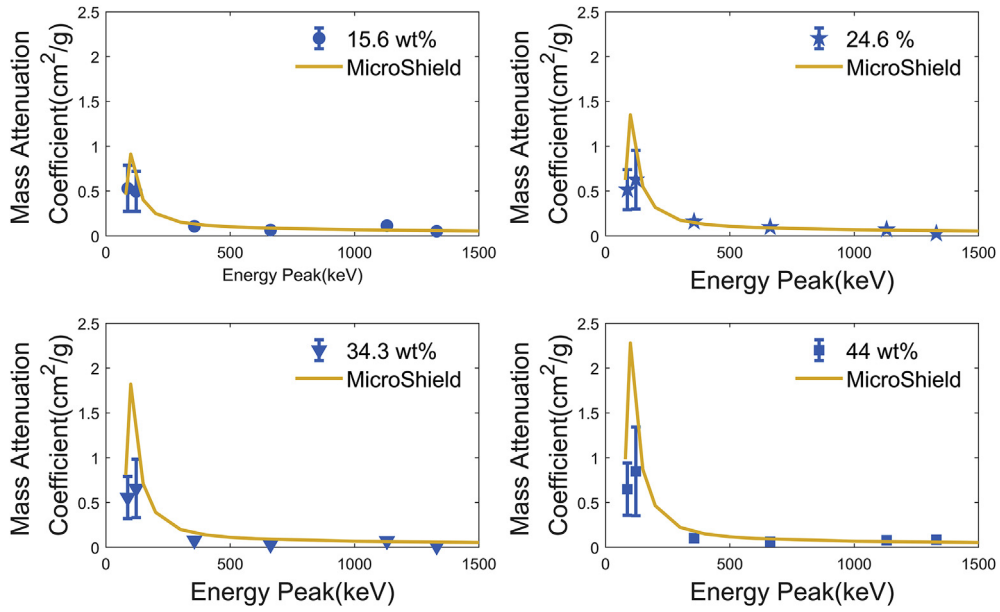

Fig. 6. Mass attenuation coefficient of PMMA composites with different loadings of Bi_2O_3 based on experiments and MicroShield software.

caused by a pyramidal diamond indenter with D1 = 150.1 μm and D2 = 166 μm. Thus, the value of hardness is calculated based on the load force from the indenter and diameters of the obtained rhombic cross section. As shown in Fig. 7, the Knoop micro-hardness is increasing with the increasing contents of Bi_2O_3 particles. It should be noted that there is a slight drop with the increase of Bi_2O_3 particles in the initial stage, which may be the result of poor contact between Bi_2O_3 particles and the PMMA matrix [20]. The overall results show that the Knoop hardness increases accordingly with the higher loading of Bi_2O_3 particles.

4. Conclusion

Unlike the thermal curing method, UV curing represents fast polymerization on the order of minutes at room temperature, which holds the potential for the rapid manufacturing of radiation shielding materials. In the present investigation, samples with 0.94g TPO achieved a curing time of 9 min. Different Bi_2O_3 contents

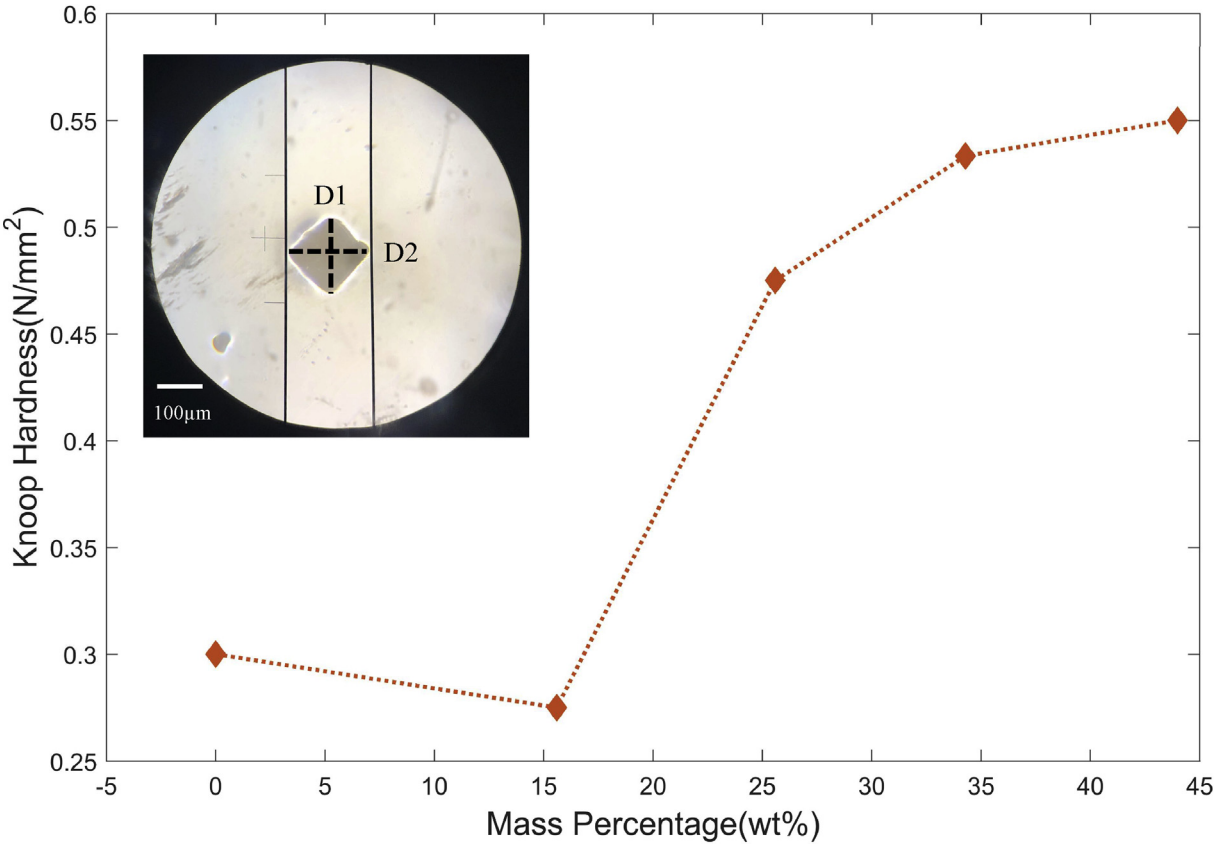

Fig. 7. Knoop hardness measurement of PMMA composite with 0–44.0 wt% Bi_2O_3 particles.

from 0 wt% to 44.0 wt% have been added into PMMA solution, and PMMA/Bi_2O_3 composites showed a better gamma shielding ability than pure PMMA for gamma energy up to 1000 keV. The Knoop hardness measurement also demonstrates that the mechanical hardness increases with higher loading of Bi_2O_3 particles. These results indicate that the fast UV curing method has a great potential for the rapid-manufacturing of radiation shielding materials with excellent mechanical and shielding properties. Further research could focus on the thermal property study of PMMA/Bi_2O_3 shielding materials. Advanced stirring methods could be further explored to improve the overall homogeneity of particles within plastic composites.

Declaration of competing interest

The authors declare that they have no known competing financial interests or personal relationships that could have appeared to influence the work reported in this paper.

Acknowledgments

The authors thank the support from the U.S. Nuclear Regulatory Commission (NRC). We also would like to thank Dr. Korukonda Murty of the Department of Nuclear Engineering from North Carolina State University for kindly sharing the Micro-indentation equipment. The authors also appreciate the valuable discussion and help from Dr. Hanhan Zhou of the Analytical Instrumentation Facility (AIF) in NCSU. X-ray Tomography measurements were performed at the AIF of North Carolina State University, which is supported by the State of North Carolina and the National Science Foundation (award number ECCS-1542015). AIF is a member of the North Carolina Research Triangle Nanotechnology Network (RTNN), a site in the National Nanotechnology Coordinated Infrastructure (NNCI).

Appendix A. Supplementary data

Supplementary data related to this article can be found at https://doi.org/10.1016/j.net.2020.04.026.

References

[1] Michael Fusco, Multilayer Protective Coatings for High-Level Nuclear Waste Storage Containers, PhD dissertation, North Carolina State University, 2016.
[2] V. Udmale, D. Mishr, R. Gadhave, D. Pinjare, R. Yamgar, Development trends in conductive nano-composites for radiation shielding, Orient. J. Chem. 29 (3) (2013) 927–936, https://doi.org/10.13005/ojc/290310.
[3] M.E. Mahmoud, A.M. El-Khatib, M.S. Badawi, A.R. Rashad, R.M. El-Sharkawy, A.A. Thabet, Recycled high-density polyethylene plastics added with lead oxide nanoparticles as sustainable radiation shielding materials, J. Clean. Prod. 176 (2018) 276–287, https://doi.org/10.1016/j.jclepro.2017.12.100.
[4] H. Wang, H. Zhang, Y. Su, T. Liu, H. Yu, Y. Yang, B. Guo, Preparation and radiation shielding properties of Gd2O3/PEEK composites, Polym. Compos. 36 (4) (2015) 651–659, https://doi.org/10.1002/pc.22983.
[5] S. Nambiar, J.T. Yeow, Po,ymer-composite materials for radiation protection, ACS Appl. Mater. Interfaces 4 (11) (2012) 5717–5726, https://doi.org/10.1021/am300783d.
[6] Winter, H., Brown, A. L., & Goforth, A. M., Bismuth-Based Nano-and Micro-particles in X-Ray Contrast, Radiation Therapy, and Radiation Shielding Applications. Bismuth: Advanced Applications and Defects Characterization, intechopen, DOI: 10.5772/intechopen.76413.https://doi.org/10.5772/intechopen.76413.
[7] N. Vana, M. Hajek, T. Berger, M. Fugger, P. Hofmann, Novel shielding materials for space and air travel, Radiat. Protect. Dosim. 120 (1–4) (2006) 405–409, https://doi.org/10.1093/rpd/nci670.
[8] T. Bel, C. Arslan, N. Baydogan, Radiation shielding properties of poly (methyl methacrylate)/colemanite composite for the use in mixed irradiation fields of neutrons and gamma rays, Mater. Chem. Phys. 221 (2019) 58–67, https://

doi.org/10.1016/j.matchemphys.2018.09.014.
[9] A. Endruweit, M.S. Johnson, A.C. Long, Curing of composite components by ultraviolet radiation: a review, Polym. Compos. 27 (2) (2006) 119–128, https://doi.org/10.1002/pc.20166.
[10] A. Singh, Radiation processing of carbon fibre-reinforced advanced composites, Nucl. Instrum. Methods Phys. Res. Sect. B Beam Interact. Mater. Atoms 185 (1–4) (2001) 50–54, https://doi.org/10.1016/S0168-583X(01)00753-4.
[11] V.J. Lopata, C.B. Saunders, A. Singh, C.J. Janke, G.E. Wrenn, S.J. Havens, Electron-beam-curable epoxy resins for the manufacture of high-performance composites, Radiat. Phys. Chem. 56 (4) (1999) 405–415, https://doi.org/10.1016/S0969-806X(99)00330-8.
[12] C. Decker, UV-radiation curing chemistry, Pigment Resin Technol. 30 (5) (2001) 278–286, https://doi.org/10.1108/03699420110404593.
[13] A. Udagawa, Y. Yamamoto, Y. Inoue, R. Chûjô, Dynamic mechanical properties of cycloaliphatic epoxy resins cured by ultra-violet-and heat-initiated cationic polymerizations, Polymer 32 (15) (1991) 2779–2784, https://doi.org/10.1016/0032-3861(91)90108-U.
[14] P. Kaur, K.J. Singh, S. Thakur, P. Singh, B.S. Bajwa, Investigation of bismuth borate glass system modified with barium for structural and gamma-ray shielding properties, Spectrochim. Acta Mol. Biomol. Spectrosc. 206 (2019) 367–377, https://doi.org/10.1016/j.saa.2018.08.038.
[15] P. Kaur, K.J. Singh, S. Thakur, Evaluation of the gamma radiation shielding parameters of bismuth modified quaternary glass system, AIP Conference Proceedings (1953), 090031, https://doi.org/10.1063/1.5032878 (2018).
[16] N. Chanthima, J. Kaewkhao, Investigation on radiation shielding parameters of bismuth borosilicate glass from 1 keV to 100 GeV, Ann. Nucl. Energy 55 (2013) 23–28, https://doi.org/10.1016/j.anucene.2012.12.011.
[17] G.F. Knoll, Radiation Detection and Measurement, John Wiley & Sons, 2010.
[18] J. Lopez, Microhardness testing of plastics: literature review, Polym. Test. 12 (5) (1993) 437–458, https://doi.org/10.1016/0142-9418(93)90016-I.
[19] W. Poltabtim, E. Wimolmala, K. Saenboonruang, Properties of lead-free gamma-ray shielding materials from metal oxide/EPDM rubber composites, Radiat. Phys. Chem. 153 (2018) 1–9, https://doi.org/10.1016/j.radphyschem.2018.08.036.
[20] G. Pinto, A. Jiménez-Martín, Conducting aluminum-filled nylon 6 composites, Polym. Compos. 22 (2001) 65–70, https://doi.org/10.1002/pc.10517.